Linking microwave heating of aqueous spheres to morphology-dependent resonances

Cite as: AIP Advances **12**, 115216 (2022); https://doi.org/10.1063/5.0122773
Submitted: 27 August 2022 • Accepted: 25 October 2022 • Published Online: 11 November 2022

Yuchen Song, John Shafe-Purcell and Aaron D. Slepkov

Linking microwave heating of aqueous spheres to morphology-dependent resonances

Cite as: AIP Advances 12, 115216 (2022); doi: 10.1063/5.0122773
Submitted: 27 August 2022 • Accepted: 25 October 2022 •
Published Online: 11 November 2022

Yuchen Song, John Shafe-Purcell, and Aaron D. Slepkov[a)]

AFFILIATIONS

Department of Physics & Astronomy, Trent University, Peterborough, Ontario K9L 0G2, Canada

[a)]Author to whom correspondence should be addressed: aaronslepkov@trentu.ca

ABSTRACT

It was recently suggested that the sparking of grape dimers in microwave ovens is due to the interaction of morphology-dependent resonances in aqueous spheres. However, evidence for microwave resonances in individual grape-sized aqueous spheres has remained weak and is open to interpretation. In this work, we provide new experimental evidence for size-dependent resonances in hydrogel spheres via calorimetric measurement of the electromagnetic energy absorbed by hydrogel spheres under microwave irradiation. Using finite-element simulations, we predict the resonant behavior of grape-sized aqueous spheres and further explore the differences between mode intensities in free-space and various *in situ* positions of a microwave oven. The lowest morphology-dependent resonance—a magnetic dipolar mode—is experimentally confirmed, appearing at the predicted diameter of ~1.35 cm. Finally, experimental evidence for higher order modes in larger spheres is suggestive but remains unresolved.

I. INTRODUCTION

The formation of plasma between grape dimers in a microwave oven has been a peculiarity that eluded an adequate explanation for decades following its discovery.[1–4] In aiming to explain this phenomenon, Khattak *et al.* found that morphology dependent resonances (MDRs) within each spherical grape "monomer" can constructively interfere in a region between the two spheres, creating a super-focused hotspot of the order of $\lambda_0/100$, where λ_0 = 12.2 cm is the free-space wavelength for 2.45 GHz waves.[2] It was posited that this electromagnetic hotspot is the cause of the sparking. More recently, Lin *et al.* observed similar sparking of aqueous dimers at a much lower frequency of 27 MHz, a condition that seemingly precludes formation of optical resonances.[4] Taken together, these works reopen questions not only about the precise mechanism responsible for the formation of plasma but, importantly, also about the evidence for the excitation of electromagnetic resonances in grape-sized aqueous spheres at microwave frequencies.

Previous thermal imaging evidence for MDRs was limited in its explanatory ability by the fact that it only records the surface temperature of the object being imaged and by the limited range of object sizes that have been visualized.[2,3] Thus far, thermal imaging has only provided qualitative and circumstantial evidence for the presence of MDR, where it is most useful for visualizing the structure of the EM modes inside the spheres by imaging cross-sectional temperature distributions after bisection. In this work, we provide complementary evidence for the existence of MDRs in aqueous spheres through the measurement of size-dependent bulk heating of microwave-irradiated hydrogel spheres.

As a route to independent quantitative evidence of microwave MDRs in aqueous spheres, we adopt a calorimetric approach whereby the electromagnetic energy absorbed during microwave irradiation is mapped across the relevant size scale of hydrogel spheres. In this approach, the thermal energy added to the aqueous spheres by absorption of 2.45 GHz microwaves is used as a proxy for the volume-averaged electromagnetic (EM) energy density inside the object during irradiation. Employing COMSOL software, we use finite element method (FEM) simulations to visualize the internal EM distribution of the irradiated hydrated beads at the microwave frequency, identifying optical resonances in aqueous spheres at different diameters. The excess thermal energy measured by calorimetry is then compared to the integrated EM energy density predicted by FEM simulations for a given bead size, yielding strong

evidence for the excitation of the fundamental MDR in grape-sized aqueous spheres.

II. MATERIALS AND METHODS

A. Materials

Amorphous spheres of hydrated sodium polyacrylate, colloquially known as "water beads" or "hydrogel beads," were used analogous to spheres of pure water. Stacked styrofoam cups were used as insulated calorimetry vessels. The temperature was measured with negative temperature coefficient (NTC) thermistors (MF58, 100 kΩ at 25 °C), providing 0.01 °C measurement precision. An Arduino Nano microcontroller was used for data acquisition and control. Masses were measured using a digital scale with a precision of 0.01 g. Microwave irradiation was performed within a conventional microwave oven (Danby DBMW0720BBB 700W). Thermal images were captured with a Teledyne FLIR T540 camera. Simulations were performed with COMSOL Multiphysics version 5.3.

B. Water bath calorimetry

Hydrogel spheres of preselected sizes are prepared by soaking dehydrated beads in a prescribed amount of water. The size of the water beads increases during hydration until the water is fully absorbed and the spheres reach hydrostatic equilibrium. Dry beads have a mass of 0.02 g and a diameter of 0.32 cm. The smallest water bead to be considered sufficiently hydrated for our experiments measured 0.03 g, with a corresponding diameter of 0.36 cm. The bead diameters chosen for the experiment thus ranged from ~0.40 to 4.00 cm, with a targeted sampling size resolution of roughly 0.10 cm.

Prior to performing the experiment, the water for calorimetry was stored in a reservoir and allowed to thermalize with the environment, as were the water beads. The size of each bead was determined immediately prior to irradiation by measuring its mass (m_b) on a digital scale and estimation of the diameter of an aqueous sphere with the same mass via

$$d = \left(\frac{6m_b}{\pi\rho}\right)^{1/3}, \tag{1}$$

where $\rho = 1.0$ g/cm^3 is taken to be the density of the hydrated bead. This approximation is valid because the water beads are up to 99.8% water by mass when fully hydrated and sodium polyacrylate has an approximate density of 1.2 g/cm^3, which thus contributes negligibly to the uncertainty in the measurement. To assure complete submersion in water for each bead size, the calorimetric ratio—the mass of water verses the mass of the bead—was varied from 10:1 for the smallest beads to 1:1 for the largest beads. The temperature of the water in the calorimeters was measured and logged in 0.1 second intervals, starting ~50 s prior to (post-irradiation) bead submersion.

All beads were irradiated at full power. However, the heating time for beads of different sizes varied iteratively, based on the effect of irradiation on the beads. For example, while most beads required 5 s of irradiation to allow for a measurable temperature change, other beads were observed to crack or burst after ~4 s and thus were only heated for 3 s in subsequent runs. Calibration of irradiation times using fixed volumes of liquid water established the linearity of EM energy fluence with irradiation time, thus allowing for normalization of absorbed energy density per unit time.

After irradiation, a bead was promptly removed from the oven and placed inside the calorimeter vessels with a predetermined quantity of water of known mass and temperature.

Logging of the temperature measurement was started a few seconds before the water bead was added to the calorimeter to establish the initial temperature, T_i. Once submerged, the temperature rise of the bath was monitored, and the final asymptotic temperature, T_f, was recorded as the point at which the slope of the temperature curve fell below 0.001 °C/s. This criterion allows for variable thermalization times for different masses of water and beads. The time-averaged thermal energy added to each bead was adjusted by the irradiation time, t_{irr}, according to the following equation:

$$\Delta Q = \frac{C(m_{H2O} + m_b)(T_f - T_i)}{t_{irr}}, \tag{2}$$

where C is the specific heat of water and m_{H2O} is the mass of water in the reservoir. Ultimately, $\Delta Q/m_b$ is estimated as a proxy for the volume-averaged electric-field energy density inside a given bead. An example of the resulting data curves for calorimetry runs of two (different sized) beads is presented in Fig. 1.

An unexpected artifact hindered the measurement of absorbed microwave energy in the smallest beads. The water sorption process is endothermic in polyacrylate hydrogel.[5] Thus, all but the

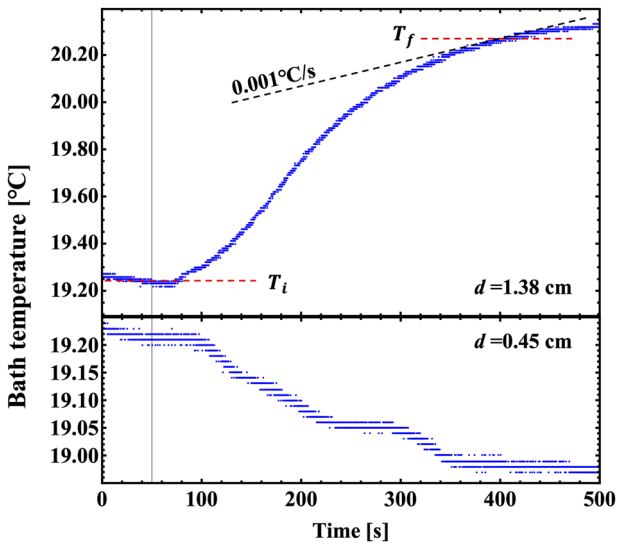

FIG. 1. Raw water bath calorimetry data measured for a resonant, d = 1.38 cm, bead (top plot) and a small, d = 0.45 cm, bead (bottom plot). Both beads were irradiated at full power for 5 s, followed by thermalization in 30.0 g of calorimeter water. The temperature of the water bath was measured at 0.15 s intervals, starting ~50 s prior to addition of the post-irradiated bead (indicated by the thin vertical line). The initial temperature, *Ti*, is measured when the bead is added to the bath, and the final temperature, *Tf*, is determined when the rate of temperature change falls below 0.001 °C/s. A temperature decrease arising from endothermic hydration in the smallest beads dominates any added microwave energy, as seen in the bottom plot.

largest beads absorb thermal energy from the water bath as calorimetry is being performed. This leads to an initial reduction in bath temperature, as can be seen in Fig. 1. This artifact results in an underestimation of the absorbed microwave energy in the smallest beads. A quantitative estimate of the effect of hydration on the calorimetric measurement of microwave heating was conducted by a series of runs with un-irradiated beads of various sizes. In doing so, we find that temperature changes due to the endothermic sorption process were negligible for beads of diameters greater than ~0.75 cm.

C. FEM simulation

The hydrated monomer is simulated as a sphere of water, with a mass density of ρ = 1.0 g/cm^3 and a relative complex permittivity ε_r = 80.12 + i9.49 at 20 °C and 2.45 GHz.[6,7] For simplicity, the dielectric properties of the bead are assumed to be uniform throughout the object, and thus, they are independent of the localized temperature gradient formed during irradiation. Air, with relative permeability and permittivity of unity (i.e., $\mu_r = \varepsilon_r = 1$), is modeled as the transmission medium. A 3D model of the microwave resonance cavity (of dimensions 28 × 26 × 17.5 cm^3), including the location and size of the irradiation waveguide port, was created in COMSOL. The incident light was presumed to comprise the port's fundamental TE (1,0) mode at 2.45 GHz, and the oven walls were simulated with reflective boundary conditions. The position of a hydrogel bead in two arbitrary and distinct positions within the microwave oven volume was simulated, denoted by locations 1 and 2. Alternatively, free-space irradiation was also simulated, with large area plane-wave incidence, with the dielectric object at the center of the simulation volume, and under fully absorbing boundary conditions. These models are shown schematically in Fig. 2.

III. RESULTS AND DISCUSSION

The internal volume-averaged EM energy density for beads simulated in free space is shown for a range of sizes in Fig. 3. Size parameterization is presented using both bead diameter and *size parameter*, *s*. This size parameter is a ratio between the diameter of the scatterer and the incident wavelength. It relates to how many wavelengths span the outer circumference of the object, as defined by

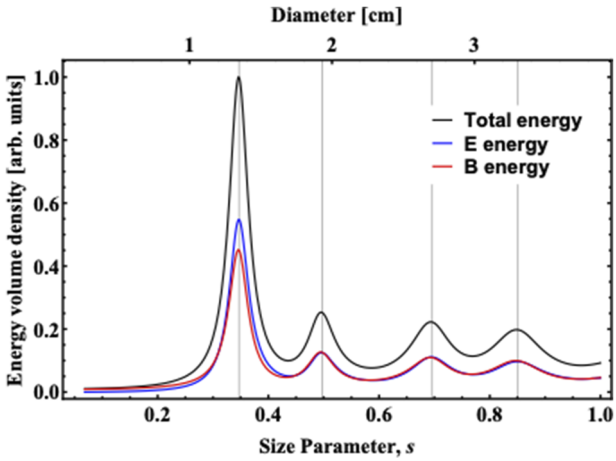

FIG. 3. Simulated spectrum of the internal resonances in hydrogel spheres irradiated at 2.45 GHz in free space, visualized through internal volume-averaged EM energy densities. The vertical lines mark the first four resonance modes obtained in the bead at size parameters s = 0.35, 0.50, 0.70, and 0.85 (i.e., diameters of 1.35 cm, 1.92 cm, 2.7 cm, and 3.3 cm, respectively). The total energy density (black) is a sum of the electric (blue) field and magnetic (red) field energy densities.

$$s \equiv \frac{\pi d}{\lambda_0}, \tag{3}$$

where d is the diameter of the object and λ_0 is the incident wavelength. The usefulness of parameterizing the object size with s rather than the diameter is that normalization of the object's size to that of the wavelength allows for more direct comparison of resonant scattering phenomena at other frequencies and sizes, such as, for example, nanoparticles at visible wavelengths[8,9] or high-index ceramics at microwave frequencies.[10] As shown in Fig. 3, the first four resonances are found at s = 0.35, 0.50, 0.70, and 0.85 corresponding to bead diameters of 1.35, 1.9, 2.7, and 3.3 cm, respectively. The primary resonance arises at a diameter of 1.35 cm, which closely matches the size of grapes reported by Khattak *et al.*[2] This mode emerges as being significantly stronger than the next three higher-order modes in larger spheres.

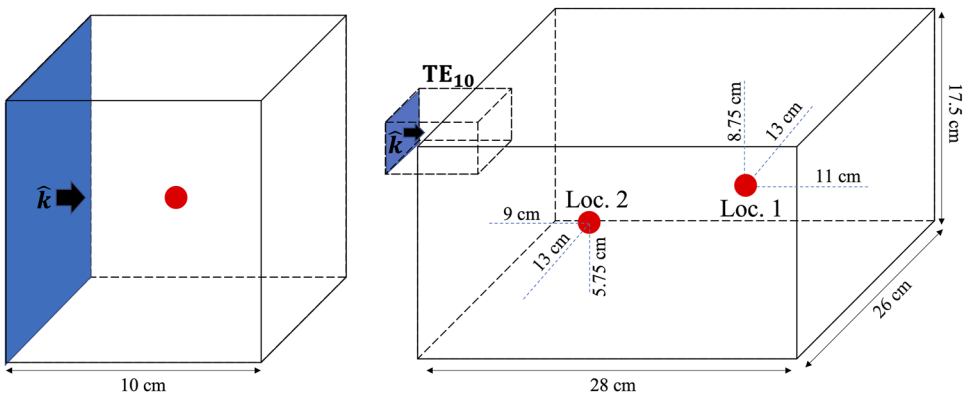

FIG. 2. Simulation schematics for free-space (left) and microwave oven (right) models. Microwave radiation at a frequency of 2.45 GHz is introduced through the boundary (blue surface) along the propagating vectors, ***k***. Free-space boundaries are modeled as perfect absorbers, while oven boundaries are modeled as conductive reflectors.

Each of the resonant modes has a particular 'character,' as defined by the distribution of electric and magnetic fields. These can be visualized by looking at the shapes of the electric and magnetic fields (or energy) internal to the objects. For example, in Fig. 4, we present the simulated EM energy density maps in the plane perpendicular to the wave propagation vector for the four resonant modes identified via peaks in the volume-averaged energy density (of Fig. 3). The shape of the electric and magnetic energy density maps confirms the expectation that the four fundamental modes correspond to, in order of increasing size, a magnetic dipole, electric dipole, magnetic quadrupole, and electric quadrupole mode, respectively.[9] We find that the total electromagnetic energy distribution in the lower-order modes is less intense but, importantly, more extensive (i.e., spanning a greater proportion of the volume). After being integrated over the whole volume, the centrally located high intensity energy distribution in the higher order modes leads to an overall lower energy per unit volume than in the lowest order modes. This means that while thermal imaging could be expected to show higher localized peak temperatures in larger resonant beads, whole-volume calorimetry would show a greater volume-averaged energy transfer to the smaller resonant beads, consistent with the trend in Fig. 3.

As can be seen in Fig. 4, the total electromagnetic energy density is largely radially symmetric irrespective of the electromagnetic character of the individual mode. However, each of the electric and magnetic energy maps is not necessarily radially symmetric. For example, as a magnetic-dipolar mode, the lowest-order mode displays a quasi-radially-symmetric central distribution of magnetic field, along with a toroidal electric field concentration. Depending on the actual cutting plane (from which thermal imaging might be obtained, for example), a map of the electric energy distribution for this mode would appear either as a toroid or as two lobes. The plane chosen for display in Fig. 4, for example, yields a vertically arranged double lobe. The higher order modes likewise oscillate between quasi-radial electric and magnetic energy density maps and lobed magnetic and electric energy density maps. Both the thermal imaging work and calorimetry work presented here are predicated on the assumption of clear correspondence between the electromagnetic field distribution and the temperature map in the objects. Simplistically, one might assume that all absorption, and thus all heating, results from the imaginary component of the water's electric susceptibility and negligibly from the magnetic permittivity.[11] Thus, we might expect the temperature map to closely represent the electric field energy distribution rather than the total EM energy map. In practice, however, as seen in Fig. 4, the temperature maps experimentally obtained from the equatorial cutting planes look much more like the total energy density maps for the four modes, that is, they are largely radially symmetric. Nonetheless, this ambiguity in the interpretation of the thermal images remains an important matter for future investigation. The thermal maps do, however, show another telltale sign of MDRs: In confirmation of the predictions from the total EM energy maps shown in Fig. 4, the thermal images shown in Fig. 5 reveal an increasing level of resonant confinement with increasing modal order. The resonance in the smallest object is seen to span a much larger proportion of the equatorial plane than does the resonance in the largest object. Ultimately, thermal imaging only provides a two-dimensional snapshot that further motivates the whole-object thermal assay that can be provided by calorimetry.

The electromagnetic environment in a microwave oven is expected to be very different from that for idealized free space plane-wave incidence. Without strong absorption in either the oven interior or walls, the chamber can act as a resonant cavity of sorts in which the position of the irradiated object relative to various EM hotspots can play a significant role in the heating dynamics.[12] Our simulations suggest that, as expected, the location within the

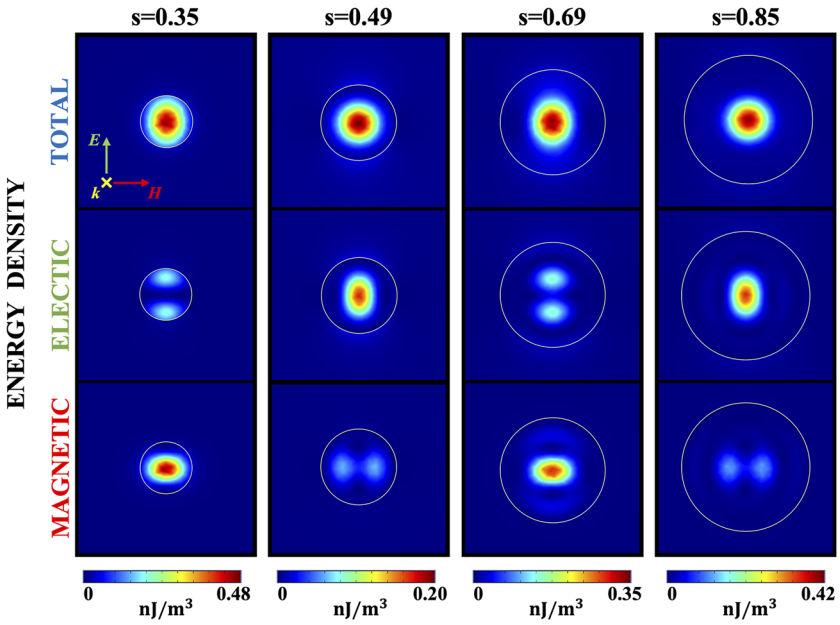

FIG. 4. Simulated EM energy distributions at the equatorial plane of the first four resonances in beads irradiated in free space. Black circles are object circumferences, to scale. The total EM energy, shown in the top row, is a sum of the magnetic (bottom row) and electric (middle row) field energies. Note that the central total energy hotspot occupies a larger proportion of the volume in the lower order resonances (in smaller beads) than it does in the higher order resonances (in larger beads).

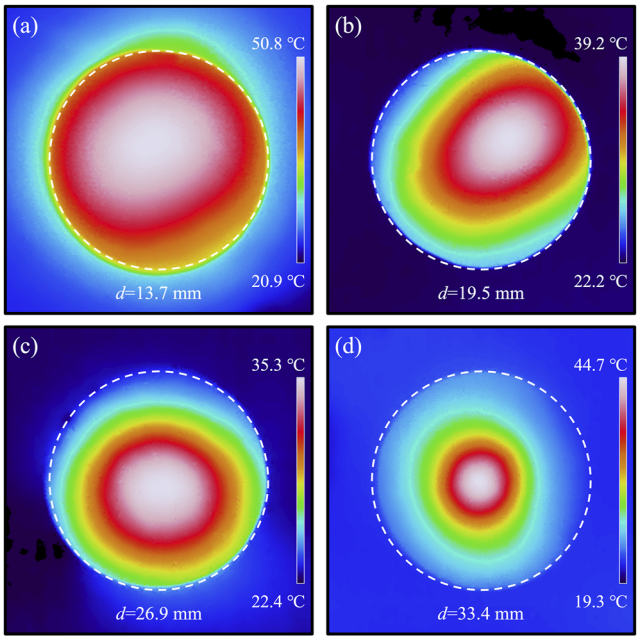

FIG. 5. Thermal images from equatorial planes of irradiated hydrogel beads at the four fundamental resonant sizes. Bead sizes: (a) 13.7 mm diameter (s = 0.35); (b) 19.5 mm diameter (s = 0.50); (c) 26.9 mm diameter (s = 0.69); (d) 33.4 mm diameter (s = 0.86). Each bead was irradiated on full power for 5 s, promptly removed from the microwave oven, cut in half, and imaged within 8–15 s after irradiation. Note the progression of relative energy concentration (maximum temperature) from the smallest in (a) to the largest bead in (d).

microwave oven has little influence on the resonant frequency but strong influence on the resonant amplitude of any given mode.[10] Certain locations within the oven cavity modes may be partially or fully suppressed. An example of this is seen in Fig. 6, where the s = 0.70 mode intensity is diminished in the oven compared to that of the free-space simulation (of Fig. 3). This reduction in resonant amplitude manifests as a slight shift in the peak frequency in location 1 and in complete suppression of the resonance in location 2. The altering of resonant amplitudes in microwave vs free-space irradiation may explain why the peak temperatures recorded in the thermal images do not strictly follow the quantitative maximum energy densities shown in the simulated mode maps for free-space irradiation. For example, while the thermal maps of Fig. 5 confirm mode-map predictions (Fig. 4) of highest peak temperatures in the s = 0.35 and s = 0.85 modes, the free-space model incorrectly predicts significantly higher peak temperatures in the s = 0.70 mode compared to the s = 0.50 mode.

Calorimetry measurements show strong variation in absorbed electromagnetic energy as a function of bead size. Figure 7 shows the normalized energy per unit mass per unit time absorbed by water beads of various sizes at two different locations within the oven. In both cases, we observe a prominent peak at a diameter of 1.35 cm (s = 0.35), which closely matches that predicted by simulations. Note that this is also approximately the size of the grapes investigated by Khattak *et al.,* which led to the super-focused hotspot in the gap between the grape dimers.[2] This provides

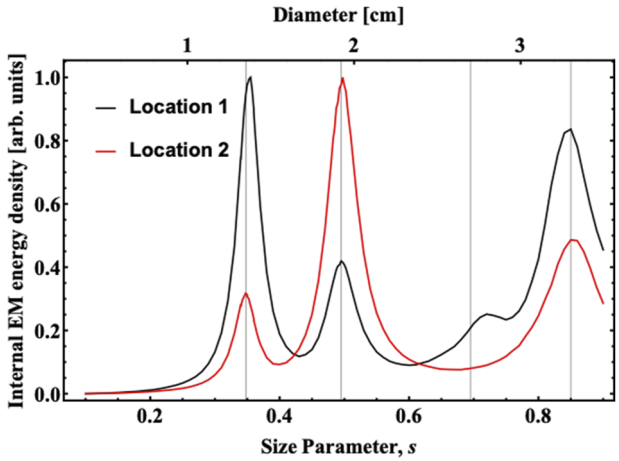

FIG. 6. Simulated spectrum of the internal resonances in hydrogel spheres irradiated at two unique locations *in situ* of a microwave oven, visualized through internal EM energy densities. The vertical lines correspond to the four resonances in the free-space simulation. The coordinates of locations 1 and 2, relative to the microwave incidence waveguide port, are shown in Fig. 1.

strong supporting evidence for MDRs in grape-sized aqueous spheres.

Beyond the lowest resonance mode, the peaks at larger diameters are suggestive but ultimately unresolved. One reason why higher order modes are difficult to resolve experimentally is that the signal-to-noise ratio is inversely proportional to the bead diameter, and the absorbed EM energy is not sufficiently high in large beads to exceed the noise floor, that is, as resonant hotspots become increasingly confined as a function of size, the per-mass average absorbed energy remains small. Increasing irradiation time also increases the maximum local temperature, which can exceed the local boiling

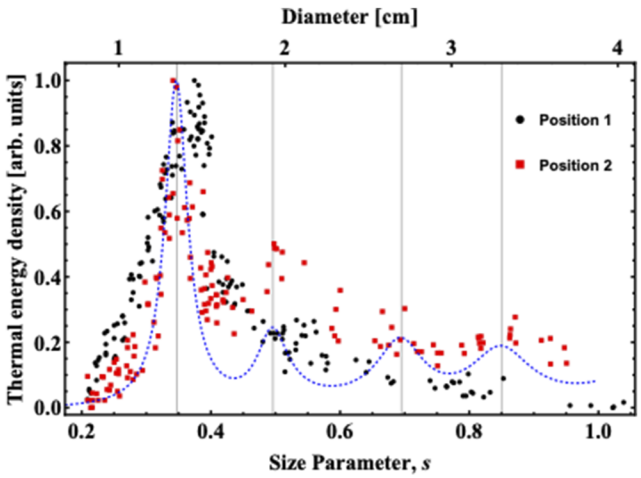

FIG. 7. Calorimetric measurement of normalized electromagnetic energy density absorbed by irradiated beads of various sizes. The trials from two distinct positions in the oven are shown. The blue dotted curve is the simulated free-space spectrum overlaid as a guide to the eye.

temperature and thus the structural integrity of the object. Future studies could perhaps resolve these higher order peaks by increasing the signal-to-noise ratio by irradiating the beads under more controlled conditions than a conventional microwave oven (noise reduction) and/or irradiating large beads for a longer duration at lower power (signal enhancement).

As suggested by the simulations and confirmed in our experiments, the use of an enclosed microwave oven for irradiation makes it challenging to control the conditions under which the beads are heated since the electromagnetic field distribution in the oven is nonuniform. This negatively impacts the repeatability of results as it is difficult to both precisely position the beads in the enclosure and to compare results between devices. Moreover, the complex dielectric properties of water exhibit significant and nonlinear temperature dependence,[7,13] which means that for better quantitative agreement with simulation, a dynamical approach needs to be adopted to account for both the temporal and spatial evolution of temperature gradients formed during irradiation.[14]

IV. SUMMARY

We developed a calorimetric approach to confirm the presence of morphology-dependent resonances in aqueous spheres exposed to 2.45 GHz microwaves. Our approach presumes that size-dependent bulk heating of water beads is a suitable proxy for the volumetric internal EM energy density established in the objects during irradiation. FEM simulations predict peaks in the volume-averaged internal EM energy density at sizes corresponding to spherical harmonic modes in the bead structure, with a primary magnetic-dipole-like mode at a bead diameter of 1.35 cm. Our calorimetric results yield a prominent resonance in the bulk heating of beads of this size, thus adding strong support to a key portion of the hypothesis that optical resonances play a role in the heating of aqueous objects and the sparking of aqueous dimers in conventional microwave ovens.

ACKNOWLEDGMENTS

This study was supported by an NSERC Discovery grant (Grant No. RGPIN/4491-2018). We thank Miao Hu for formative discussions on the theory of MDRs in aqueous spheres and for confirmation of preliminary COMSOL simulation findings.

AUTHOR DECLARATIONS

Conflict of Interest

The authors have no conflicts to disclose.

Author Contributions

Yuchen Song and John Shafe-Purcell contributed equally to this work.

Yuchen Song: Data curation (equal); Investigation (supporting); Methodology (equal); Software (lead); Visualization (equal); Writing – original draft (lead); Writing – review & editing (equal). **John Shafe-Purcell**: Conceptualization (supporting); Data curation (equal); Investigation (lead); Methodology (equal); Visualization (supporting); Writing – original draft (equal); Writing – review & editing (supporting). **Aaron D. Slepkov**: Conceptualization (lead); Funding acquisition (lead); Investigation (supporting); Methodology (equal); Supervision (lead); Visualization (equal); Writing – original draft (equal); Writing – review & editing (lead).

DATA AVAILABILITY

The data that support the findings of this study are available from the corresponding author upon reasonable request.

REFERENCES

[1] P. R. Michaud, Fun with grapes: A case study (1994) (available URL: https://web.archive.org/web/20190130194653/http://pmichaud.com/grape/. (accessed on 10 August 2022).
[2] H. K. Khattak, P. Bianucci, and A. D. Slepkov, "Linking plasma formation in grapes to microwave resonances of aqueous dimers," Proc. Natl. Acad. Sci. U. S. A. **116**, 4000–4005 (2019).
[3] A. Slepkov, "Fruit photonics and the shape of water," Phys. Today **73**, 62–63 (2020).
[4] M. S. Lin, L. C. Liu, L. R. Barnett, Y. F. Tsai, and K. R. Chu, "On electromagnetic wave ignited sparks in aqueous dimers," Phys. Plasmas **28**, 102102 (2021).
[5] R. Di Maggio, S. Dirè, E. Callone, L. Bergamonti, P. P. Lottici, R. Albatici, R. Rigon, and N. Ataollahi, "Super-adsorbent polyacrylate under swelling in water for passive solar control of building envelope," SN Appl. Sci. **2**, 45 (2020).
[6] The complex permittivity can be written as $\varepsilon_r = \varepsilon' \pm \varepsilon''$, where the choice of the sign of the imaginary component can represent either gain or absorption, depending on convention. In this work we report the value as 80.12 + i9.49 (as obtained from the proceeding source; T. Meissner *et al.*, 2004), with the plus sign denoting absorption. It is worth noting, however, an idiosyncrasy in the convention used within COMSOL such that absorption is defined using the negative sign (and gain with the positive). Thus, within COMSOL we used 80.12 – i9.49 for the permittivity of the simulated aqueous objects. We suspect that similar confusion is widespread and has likely led to many erroneous results in the extant literature.
[7] T. Meissner and F. J. Wentz, "The complex dielectric constant of pure and sea-water from microwave satellite observations," IEEE Trans. Geosci. Remote Sens. **42**, 1836–1849 (2004).
[8] X. Fan, W. Zheng, and D. J. Singh, "Light scattering and surface plasmons on small spherical particles," Light Sci. Appl. **3**, e179 (2014).
[9] A. I. Kuznetsov, A. E. Miroshnichenko, M. L. Brongersma, Y. S. Kivshar, and B. Luk'yanchuk, "Optically resonant dielectric nanostructures," Science **354**, eaag2472 (2016).
[10] P. Affolter and B. Eliasson, "Electromagnetic resonances and Q-factors of lossy dielectric spheres," IEEE Trans. Microwave Theory Tech. **21**, 573–578 (1973).
[11] C. Gabriel, S. Gabriel, E. Grant, B. Halstead, D. Michael, and P. Mingos, "Dielectric parameters relevant to microwave dielectric heating," Chem. Soc. Rev. **27**, 213–224 (1998).
[12] Z. Du, Z. Wu, W. Gan, G. Liu, X. Zhang, J. Liu, and B. Zheng, "Multi-physics modeling and process simulation for a frequency-shifted solid-state source microwave oven," IEEE Access **7**, 184726–184733 (2019).
[13] R. Buchner, J. Barthel, and J. Stauber, "The dielectric relaxation of water between 0 C and 35 C," Chem. Phys. Lett. **306**, 57–63 (1999).
[14] T. Santos, M. A. Valente, J. Monteiro, J. Sousa, and L. C. Costa, "Electromagnetic and thermal history during microwave heating," Appl. Therm. Eng. **31**, 3255–3261 (2011).